



Regular Research Manuscript

# Long-Range Inertia Prediction Considering Contemporary Evolution of Power Grid Networks

Peter Makolo<sup>1,2†</sup>, Francis Mwasilu<sup>2</sup>, Ramon Zamora<sup>1</sup> and Tek-Tjing Lie<sup>1</sup>

<sup>1</sup>Department of Electrical and Electronic Engineering, Auckland University of Technology, Auckland 1010, New Zealand

<sup>2</sup>Department of Electrical Engineering, University of Dar es Salaam, P.O. Box 33335, Dar es Salaam, Tanzania.

†Corresponding author: [makolo.peter@gmail.com](mailto:makolo.peter@gmail.com); ORCID: 0000-0002-3595-8468

## ABSTRACT

Reduced network inertia due to high penetration levels of non-synchronous generators in modern power systems is becoming a pressing issue. As a result, very quick inertial responses are observed after contingency events in networks. Due to quick inertial responses, there is a practically very limited time interval for control actions in real-time. Thus, system operators need to understand the prior inertia values to plan, control, and operate the network securely. Long-range forecasting of the network's inertia values, in contrast to short-range forecasting techniques, can pinpoint when the network is most likely to be vulnerable in a reasonable time ahead. Thus, in this research work, an improved ARIMA model (*i*-ARIMA) technique for long-range forecast inertia values in a modern network is proposed. To estimate future inertia values over a long period of time, the *i*-ARIMA model leverages strong periodic and seasonality characteristics of previous time series data. The *i*-ARIMA method is tuned for optimal values of a moving observant predictor *P*, periodicity and seasonality factor *s* and smoothing factor *n* that give the best forecasts with competitive accuracy. Rigorous evaluation and tests of the method, which are performed on the New Zealand network data using the Power Factory DigSilent platform, demonstrate that the proposed *i*-ARIMA is quicker, more reliable, more accurate, and better than other conventional forecasting methods.

## ARTICLE INFO

Submitted: Aug. 15, 2024

Revised: Nov. 14, 2024

Accepted: Dec. 11, 2024

Published: Jan. 2025

**Keywords:** Inertia Forecasting, Long-Range Forecasting, Frequency Response, and Short-range forecasting

## INTRODUCTION

### Background and motivation

For several decades, synchronous generators (SGs) have been fundamental components of power systems, traditionally used to produce active power, control frequency and voltage, and provide system inertia (Milano et al., 2018). The inertia of a power system

significantly influences its ability to remain stable during power imbalances. It plays a crucial role in mitigating fluctuations and disturbances within the first 5 seconds following a contingency (Milano *et. al.*, 2018; Zhang & Xu, 2017). Although inertia primarily affects the initial moments after a power imbalance, its role is essential for network stability.

Increasing integration of converter-based sources (CBS) such as wind and solar power and a large fleet of electric vehicles (EV), which are connected to the grid via converter-based techniques, is rapidly replacing conventional rotating machines in the contemporary grid (Ratnam *et al.*, 2020). Most of these CBS are non-synchronous generators with zero or small inertia contribution to the grid. It is important to mention that, one of the fundamental impacts of high share of converter-based sources to modern grid is the decrease of the conventional inertia from the grid. Although these CBS can be controlled to provide the so-called synthetic inertia and frequency support to boost the low inertia grid, the time variability of the total inertia is another concern to the stability of the power system to be addressed (Makolo, *et al.*, 2021b).

The fact that network inertia can be a variable quantity in the network triggered transmission system operators' (TSOs) interest in a prior understanding of the system inertia behaviour in power systems (Makolo, *et al.*, 2021b). Prior understanding of system inertia can enable power system operators (PSOs) to take the right control actions related to the system stability and operate the network securely (Du & Matevosyan, 2017). Regarding understanding the behaviour of network inertia, several methods for estimating inertia have been proposed in the body of literature. The methods are meant to comprehend the power system's inertia values. For instance, offline estimation techniques such as in (Makolo, *et al.*, 2021; Sfetkos *et al.*, 2023) are established to quantify the past inertia values when events happen in power systems for analysis purposes. This is to say, information obtained from offline inertia estimation techniques cannot be used for protection and remedial measures in real-time. For this reason, methods to estimate inertia values in real-time, such as in (Panda *et al.*, 2020; Liu *et al.*, 2020; Makolo, *et al.*, 2021a; Linaro *et al.*, 2023), are established to monitor the inertia variation in the power system and, therefore, can be used for analysis in real time.

Nevertheless, as inertia is becoming a time-dependent parameter in the power system, offline and real-time methods for inertia estimation cannot serve grid protection purposes (Kisinga *et al.*, 2024). Also, due to fast transient response, the online inertia techniques may be prone to instabilities in power systems in case of contingencies happening at low inertia, which is not predicted in the time ahead (Du & Matevosyan, 2017). Therefore, a prior understanding of network inertia well in the time ahead is important to forecast the behaviour of the power system in the long range. The reduction of total rotating inertias, which results in fast transients, needs to be forecasted in networks.

Again, synthetic inertias that are also known as virtual or digital inertias, which support frequency response in modern power systems, are becoming tradable quantities (Heylen *et al.*, 2020). Synthetic inertias are gaining popularity as they supplement conventional inertia in supporting network's frequency stability. Thus, purchasing a fixed quantity of synthetic inertia and applying it to the network is not effective and economical as the system's inertia may vary over a wide range in a year. Undetermined low inertia conditions and inadequate auxiliary frequency support services could pose a serious risk to the reliability and security of the network. For this reason, prior knowledge of the system inertia is crucial so that a minimum level of inertia can be planned, determined and purchased well in the time ahead to maintain stability, security, and reliability of the network following contingencies events. A network's minimum level of inertia should always be maintained to ensure the secure operation of the network (Heylen *et al.*, 2020). Therefore, understanding inertia values of the network for the time ahead gives the assurance of avoiding possible risks of instability in the power system. In addition, to maintain the network's minimum level of inertia, PSOs can schedule fast-frequency response services and appropriate reserves to provide appropriate

responses to the network under contingencies (Makolo, et. al., 2021b).

Consequently, appropriate methods to precisely forecast power system's inertia values are crucial to avoid threats related with extended operating times of the network with low inertia. To achieve this goal, this research proposes an algorithm for short- and long-range forecasts of network inertia. The proposed method introduces an improved ARIMA (*i*-ARIMA) algorithm. The *i*-ARIMA uses the seasonality and robust periodic patterns of past time series data to short- and long-range forecast future inertia values. *i*-ARIMA method is tuned for optimal values of moving observant predictor  $\mathfrak{P}$ , periodicity and seasonality factor  $s$  and smoothing factor  $n$ , collectively giving the best forecasts with competitive accuracy. The introduced  $\mathfrak{P}$ ,  $s$ , and  $n$  factors will be further discussed in subsequent sections. Rigorous evaluation and tests of the method, which are done on the New Zealand data, reveal the *i*-ARIMA to be quicker, more reliable, more accurate, and better than other forecasting methods.

### Existing literature analysis

With the integration of CBS into the power system, inertia estimate techniques have gained popularity. Numerous methods for inertia estimation have been thoroughly studied in the literature. Nonetheless, there hasn't been much discussion of inertia forecasting in this line of inquiry. Thus, it is critical to comprehend the significance of inertia estimation in power systems at this stage. It is clear that the power system inertia is reduced when stochastic non-synchronous generation units are substituted for conventional synchronous power plants. This tendency weakens the power system's frequency stability. Inertia estimation algorithms are necessary for frequency stability. It is essential to understand the network's inertia value to schedule power reserves and deploy quick frequency support devices to ensure frequency stability in the grid (Heylen et. al., 2020).

Plenty of techniques are proposed in the literature for power system inertia estimations. Established on the time horizon of interest, the inertia estimation techniques can be classified as offline, online and forecast techniques. These estimation methods can further be grouped into two main groups: disturbance data-based and non-disturbance data-based approaches. Within the disturbance data-based group, some methods are based on swing equations, and others are based on electromechanical wave theory. Most of the disturbance-based techniques are offline as they are post-mortem approaches (Cao et. al., 2016). For non-disturbance methods, some methods use the probing signal technique, and others use the ambient signal approach. Most later techniques are used in the online (real-time) and forecast (time-ahead) inertia estimation approaches. Most of the proposed techniques employing the swing equation approach estimate the inertia by monitoring the dynamics of active power and the resulting frequency responses. Other approaches link inertia and the generator's rotor angle together with the power mismatch in the grid.

The following offline inertia estimation techniques, which are mainly used for analytical and post-event assessment of the inertia level in the systems, are analysed. A switching Markov Gaussian model, which is a statistical-based approach, is developed in (Cao et. al., 2016). In this approach, historical time-series data are used to evaluate the network's inertia. The methods developed in (Chassin et al., 2005; Zografos et. al., 2020), which are based on the regression methodology, use real-time data of online load and generation mix for network's inertia estimation. A technique to calculate the inertia of the Great Britain (GB) network by considering the magnitude of the disturbance and frequency response in the network is shown in (Ashton et. al., 2014). On the other hand, the method presented in (Inoue et. al., 1997) uses transients of frequency measured during an event in connection with using a swing equation to estimate the inertia of the power system. However, the method is

affected by noise content in the measured frequency. The methods proposed in (Lugnani *et al.*, 2020) and (Tuttelberg *et al.*, 2018) use autoregressive moving average exogenous (ARMAX) models to estimate the system inertia.

Online or real-time inertia estimation techniques aim to get an immediate estimate of the inertia based on instantly accessible measurements of the system variables. Several different approaches are proposed in the body of literature. For instance, a method to estimate inertia in real time using data of the active power balance from a wide-area power system's measurement for large disturbances is presented in (Sun *et al.*, 2019). Another method for online inertia estimation using an injection of a supplementary probing indicator is proposed in (Zhang & Xu, 2017). In ref. by (Yang *et al.*, 2020), a recursive adaptive subspace identification algorithm is proposed to track real-time oscillation modes. The algorithm uses ambient data obtained from phasor measurement units (PMU) for inertia estimation of different areas of an interconnected network. Another ambient data-based online method for inertia estimation is proposed in ref. by (Tuttelberg *et al.*, 2018).

Generally, the post-mortem offline inertia estimation approaches have three pitfalls, as specified in (Heylen *et al.*, 2020). First, the techniques depend on network events to estimate the system inertia. This dependency must accurately understand the events' sizes, which is difficult. On top of this, not all events in the power system are suitable for inertia estimation and analytical purposes in the network (Ashton *et al.*, 2013; Makolo *et al.*, 2024). Second, the techniques also suffer the time determination problem for the event's onset. This is an important feature, as stated in (Wang *et al.*, 2020). Lastly, RoCoF is another challenge facing the accuracy of post-mortem inertia estimation techniques. The frequency oscillations and noise content after an event make it difficult to obtain error-free RoCoF (Tavakoli *et al.*, 2012).

All the offline and online methods for inertia estimation cannot adequately protect the low-inertia network from instabilities when contingencies happen. For instance, offline techniques provide a posteriori information, which can only be useful in scheduling stages but not for control actions in real-time (Carlini *et al.*, 2021). Yet, online methods for inertia estimation provide real-time estimates of inertia in the network. However, they are impractical for power system protection as the estimations are provided in real time. Given the speed of faults in the network, there is not enough time to communicate the estimated inertia to the PSOs and immediately take action to control the network in cases of low inertia values (Milano *et al.*, 2018; Makolo, *et al.*, 2021a; Heylen *et al.*, 2020). This is because there is not enough time interval to plan for fast-frequency support facilities as the responses are so quick. The only solution is to accurately forecast network's inertia values. Prior knowledge of system inertia and behaviour will allow PSOs to have a reasonable time interval for planning network's control, support, and protection (Du & Matevosyan, 2017).

Given the risks of unanticipated low network inertia conditions and the limited time for taking action after power imbalances in the network, there is an increasing need to forecast and anticipate the values of the inertia constant in the modern network (Makolo, *et al.*, 2021b; Makolo, *et al.*, 2021a; Wang *et al.*, 2020; Ujjwol *et al.*, 2017; Prakash *et al.*, 2018). Network inertia forecasting will anticipate when the grid will likely be at low inertia risk. In this way, appropriate measures can be taken well in advance to protect network stability (Makolo, *et al.*, 2021b; Heylen *et al.*, 2020; Ujjwol *et al.*, 2017). Unlike offline and online inertia estimations, this area of inertia forecasting has not been intensively researched. There are only a few proposed methods to forecast the inertia constants in power systems. Some of the methods are discussed in the subsequent paragraph.

Du & Matevosyan, (2017) proposes a new tool to forecast system inertia and evaluate the

adequacy of frequency response reserves. In this literature, the need for forecasting network inertia as an important characteristic to evaluate the operational impact of non-synchronous generating units on a power grid is justified. Besides, a short-term rotating energy forecast using a decomposable time series model approach is proposed in (Gonzalez-Longatt *et. al.*, 2020). Also, in (Prakash *et. al.* (2018), a two-stage stochastic generation including a primary frequency response planning model is presented to predict the network inertia for primary frequency response suitability over stochastic wind generation. Besides, an artificial intelligence-based technique is proposed in (Paidi *et. al.*, 2020). In this technique, inertia in a power system with a high penetration of wind power plants is forecasted.

Yet, the proposed inertia forecasting methods discussed in the previous paragraphs have some limitations. The method proposed in (Carlini *et. al.*, 2021) focuses more on online inertia estimation, enhanced by a prediction method for a very short time ahead. System monitoring data can be used to improve the method for long-range forecasting of inertia values in the network. Furthermore, the method proposed by (Prakash *et. al.*, 2018) fails to justify the accuracy of the claimed one-day prediction on system inertia. Again, the one-hour and three-hour time-ahead predictions of inertia in (Gonzalez-Longatt *et. al.*, 2020; Du & Matevosyan, 2017) are relatively short for reliable planning, especially for stability control in large power systems comprising large power plants. Large power plants may take a reasonably long time to start and synchronise in the network. It is possible to extend the forecasting to a longer time ahead. Moreover, the method proposed in (Paidi *et. al.*, 2020) is based only on simulation data. Its application accuracy on real network data is not justified. There is a need to justify the proposed method based on real network data.

### Novelties and organization of the paper

The contributions of the method proposed in this paper are threefold. Firstly, the proposed

method introduces the *i*-ARIMA algorithm that uses resilient periodic patterns and past time series data seasonality to long-range forecast inertia values. Secondly, the method uses moving observant predictor  $\mathfrak{P}$  to improve the accuracy of the short-range forecasts. Lastly, it combines optimal values of moving observant predictor  $\mathfrak{P}$ , periodicity and seasonality factor  $\mathfrak{s}$  and smoothing factor  $\mathfrak{n}$  at different lags  $\mathfrak{k}$ , giving the best long-range inertia forecasts with competitive accuracy.

The rest of this paper is organised as follows: Section 2 presents the theoretical background of this research work. The role of inertia in modern network stability, the impact of CBS and the role of synthetic inertia are discussed in this section. Besides, an overview and application of the ARIMA model in forecasting are presented. Section 3 explains the steps of the method proposed. The steps include model identification, inertia extraction, tracking, and forecasting. Moreover, the New Zealand network data is used to test the applicability of the proposed technique in section 4. The performance analysis of the technique is examined in section 5. Eventually, section 6 presents the conclusion of the discussion.

## CONCEPTUAL FRAMEWORK

### The role of inertia in power systems

Inertia is an important property in maintaining the stability of the power system. Conventionally, the turbine-synchronous generator rotating mass is represented as inertia that is well defined by the swing equation as given in (1) (Makolo, Zamora, et al., 2021b).

$$J \frac{d}{dt} \omega_m(t) = T_m(t) - T_e(t) \quad (1)$$

where  $J$  represents the total rotating masses' moment of inertia,  $\omega_m$  represents the mechanical rotational speed, while  $T_m$  and  $T_e$  represent the mechanical and electromagnetic torques, respectively. By converting the torques into power, the swing equation can be written in terms of power and frequency as in (2) (Heylen et al., 2020):

$$\frac{J\omega_e(t)}{p^2} \frac{d}{dt} \omega_e(t) = P_m(t) - P_e(t) \quad (2)$$

where  $\omega_e(t)$  is the instantaneous electrical rotor speed, i.e.,  $\omega_e(t) = 2\pi f(t)$ , while  $f(t)$  is the instantaneous frequency of the generator terminal voltage, and  $p$  is the pole pair number of the generator. The kinetic energy (KE) of the generator rotating masses is given by (3).

$$KE = \frac{J\omega_{e,0}^2}{2p^2} \quad (3)$$

where  $\omega_{e,0} = 2\pi f_0$  is the rated electrical rotor speed of the generator at the rated frequency  $f_0$  of the power system.

The stored kinetic energy is an important property of the power system. During the power imbalances in the power system, the stored KE is either absorbed or released by the generator to counteract the power imbalance. By so doing, the speed and frequency are instantly controlled within permissible bounds depending on the size of the power imbalance. This process is referred to as the generator's inertial response, which plays an important role in reducing the system RoCoF. Low values of RoCoF give the generator's governor the necessary time needed to regulate the turbine power to restore the power balance. When the KE is divided by the generator's nominal power ( $S_n$ ), the inertia constant  $H$  can be obtained as in (4).

$$H = \frac{KE}{S_n} = \frac{J\omega_{e,0}^2}{2p^2 S_n} \quad (4)$$

When the rotor speed  $\omega_e(t) = 2\pi f(t)$  is different from the rated rotor speed  $\omega_{e,0} = 2\pi f_0$ , (1) can be written as in (5).

$$2H \frac{d}{dt} \frac{f(t)}{f_0} = \frac{P_m(t) - P_e(t)}{S_n} \quad (5)$$

For the system with multi-generators, the swing equation of the system can be written in terms of total system inertia  $H_{sys}$  and centre of inertia frequency,  $f_{COI}$  as in (6) (Paidi *et. al.*, 2020).

$$2H_{sys} \frac{d}{dt} \frac{f_{COI}(t)}{f_0} = \frac{P_m(t) - P_e(t)}{S_n} \quad (6)$$

where the total system inertia  $H_{sys}$  is given as in (7).

$$H_{sys} = \frac{\sum_{i=1}^N H_i \times S_{n,i}}{\sum_{i=1}^N S_{n,i}} \quad (7)$$

The centre of inertia frequency  $f_{COI}$  is given by (8).

$$f_{COI} = \frac{\sum_{i=1}^N H_i \times f_i}{\sum_{i=1}^N H_i} \quad (8)$$

### The impact of renewables and the role of synthetic inertia in modern power systems

In the case of networks with high share of converter-based sources, the conventional synchronous generators are replaced, and hence, inertia is reduced in power systems (Ratnam *et. al.*, 2020). To obtain the dynamic values of inertia, the supervisory control and data acquisition (SCADA) system needs to provide the timely status of the synchronous generators in the system. By so doing, equation (7) can be modified to update the amount of network inertia. Equation (7) needs to be appropriately modified to account for the non-synchronous generators that do not add up to the KE of the system (Donnini *et al.*, 2020). To modify (7), (Donnini *et. al.*, 2020) introduces a factor  $S_R$  that accounts for the total amount of active power injected by each RE plant in the network that doesn't contribute to the total inertia of the network. Employing  $S_R$  for  $N$  number of RE plants in the network, equation (7) can be re-written in the form as presented in (9).

$$H_{sys}^{RE} = \frac{\sum_{i=1}^N H_i \times S_{n,i}}{\sum_{i=1}^N S_{n,i} + \sum_{i=1}^N S_{R,i}} \quad (9)$$

As a result of reduced conventional inertia  $H_{sys}$  of the network due to penetration of CBS, different controls of different energy storage systems and other CBS for frequency support have been gaining popularity in power systems. Supercapacitors and battery storage, for instance, have been used for fast frequency response, frequency support and inertia response. On the other hand, wind turbines have been applied for frequency support in terms of synthetic inertia and fast frequency support (Kosmecki *et. al.*, 2021). It should be noted that fast frequency response (FFR) differs from synthetic inertia in the

concept that FFR is applied during frequency deviation. In contrast, for synthetic inertia, the controller response is linked to the RoCoF to support a network with low inertia values (Donnini et al., 2020).

## THE PROPOSED METHOD TO FORECAST INERTIA IN POWER SYSTEMS

### Method overview

The proposed inertia forecasting method is an extension of the previously proposed short range inertia prediction method in (Makolo et al., 2021). The proposed method is subdivided into three main algorithms: power system model identification, inertia extraction and inertia tracking and forecasting. The algorithms are interconnected, from power model identification to inertia forecasting. **Error! Reference source not found.** (a) and (b) show in detail the generalised flow block diagrams of model identification and inertia extraction, respectively, while **Error! Reference source not found.** shows the inertia forecasting algorithm.

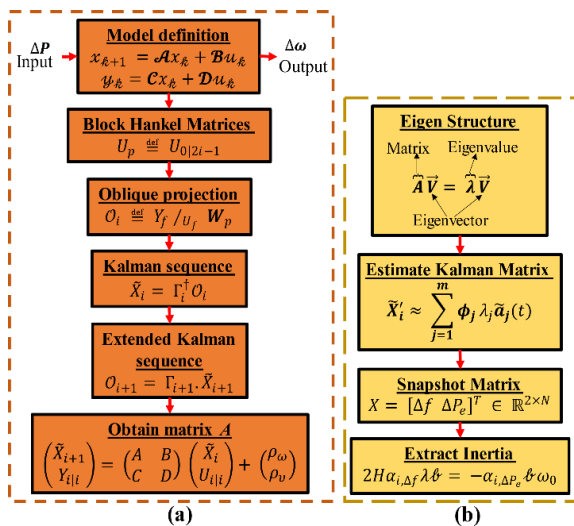


Figure 1: Algorithm flow diagrams of: (a) network model identification and (b) inertia extraction

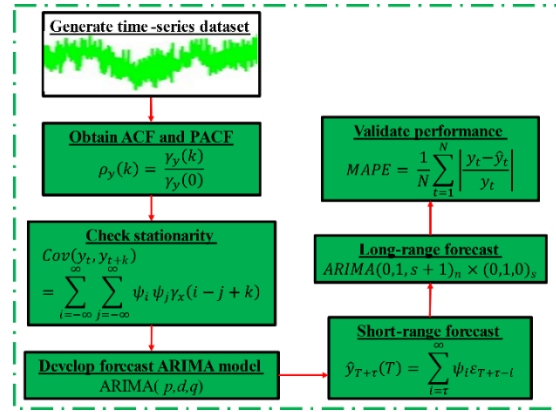


Figure 2: Flow diagram of inertia forecasting algorithm

### Model identification

Given the network measurements for the input parameter  $u_k \in \mathbb{R}^m$  and the output  $y_k \in \mathbb{R}^l$  generated by the unknown combined system of order  $n$ , the system can be represented by the state-space equation (10).

$$\begin{aligned} x_{k+1} &= Ax_k + Bu_k + w_k \\ y_k &= Cx_k + Du_k + v_k \end{aligned} \quad (10)$$

where  $u_k$  and  $y_k$  represent the inputs and outputs of the system, respectively,  $x_k$  denote the states, while  $w_k$  and  $v_k$  are the process and measurement noises. The coefficients  $A, B, C, D$  denote the system's matrices. Considering the system's noise, the combined (deterministic-stochastic) subspace identification algorithm is employed to compute the state-space model from the network's input-output data. A linear time-invariant combined with a deterministic-stochastic subspace can represent a system. Matrix  $A$  in a combined deterministic-stochastic system specifically denotes a dynamic system matrix as completely characterised by its eigenvalues (Isermann & Münchhof, 2010).

When a system has available (measured) signals  $u_k$  and  $y_k$  and  $v_k$  and  $w_k$  unknown disturbances, the system can be split into a deterministic and stochastic subsystem by splitting the state ( $x_k$ ) and output ( $y_k$ ) in a deterministic ( $\bullet^d$ ) and stochastic ( $\bullet^s$ ) components as in (11).

$$x_k = x_k^d + x_k^s$$

$$y_k = y_k^d + y_k^s \quad (11)$$

The deterministic state ( $x_k^d$ ) and output ( $y_k^d$ ) follow from the deterministic subsystem, which describes the influence of the deterministic input ( $u_k$ ) on the deterministic output as shown in (12).

$$\begin{aligned} x_{k+1}^d &= Ax_k^d + Bu_k \\ y_k^d &= Cx_k^d + Du_k \end{aligned} \quad (12)$$

The stochastic state ( $x_k^s$ ) and the output ( $y_k^s$ ) follow from the stochastic subsystem, which describes the influence of the noise sequences ( $w_k$ ) and ( $v_k$ ) on the stochastic output as depicted in (13).

$$\begin{aligned} x_{k+1}^s &= Ax_k^s + w_k \\ y_k^s &= Cx_k^s + v_k \end{aligned} \quad (13)$$

The deterministic and stochastic subsystems may have completely decoupled input-output dynamics. For this reason, the block Hankel matrices, which relate the measured input-output dynamic data, are defined as in (14) (Zhou *et al.*, 2006).

$$\begin{aligned} U_{\mathcal{P}} &\stackrel{\text{def}}{=} U_{0|2i-1} \\ &\stackrel{\text{def}}{=} \begin{pmatrix} u_0 & u_1 & u_2 & \dots & u_{j-1} \\ u_1 & u_2 & u_3 & \dots & u_j \\ \dots & \dots & \dots & \dots & \dots \\ u_{i-1} & u_i & u_{i+1} & \dots & u_{i+j-2} \end{pmatrix} \\ &\in \mathbb{R}^{li \times j} \end{aligned}$$

$$\begin{aligned} U_{\mathcal{F}} &\stackrel{\text{def}}{=} U_{i|2i-1} \\ &\stackrel{\text{def}}{=} \begin{pmatrix} u_i & u_{i+1} & u_{i+2} & \dots & u_{i+j-1} \\ u_{i+1} & u_{i+2} & u_{i+3} & \dots & u_{i+j} \\ \dots & \dots & \dots & \dots & \dots \\ u_{2i-1} & u_{2i} & u_{2i+1} & \dots & u_{2i+j-2} \end{pmatrix} \\ &\in \mathbb{R}^{li \times j} \end{aligned}$$

$$\begin{aligned} U_{\mathcal{P}}^+ &\stackrel{\text{def}}{=} U_{0|i} \\ &\stackrel{\text{def}}{=} \begin{pmatrix} u_0 & u_1 & u_2 & \dots & u_{j-1} \\ u_1 & u_2 & u_3 & \dots & u_j \\ \dots & \dots & \dots & \dots & \dots \\ u_{i-1} & u_i & u_{i+1} & \dots & u_{i+j-2} \\ u_i & u_{i+1} & u_{i+2} & \dots & u_{i+j-1} \end{pmatrix} \\ &\in \mathbb{R}^{l(i+1) \times j} \end{aligned}$$

$$\begin{aligned} U_{\mathcal{F}}^- &\stackrel{\text{def}}{=} U_{i+1|2i-1} \\ &\stackrel{\text{def}}{=} \begin{pmatrix} u_{i+1} & u_{i+2} & u_{i+3} & \dots & u_{i+j} \\ \dots & \dots & \dots & \dots & \dots \\ u_{2i-1} & u_{2i} & u_{2i+1} & \dots & u_{2i+j-2} \end{pmatrix} \\ &\in \mathbb{R}^{l(i-1) \times j} \end{aligned} \quad (14)$$

The subscripts in  $U_{0|2i-1}$ ,  $U_{0|i}$ ,  $U_{i+1|2i-1}$  denote the first and last element of the first column in the input block Hankel matrix. The subscripts “ $\mathcal{P}$ ” and “ $\mathcal{F}$ ” stand for “past” and “future” respectively. On the other hand,  $U_{\mathcal{P}}^+$  and  $U_{\mathcal{F}}^-$  are defined by shifting the border between past and future one block row down. The superscripts “+” and “-” stand for “add one block row” and “delete one block row”, respectively. The output block Hankel matrices  $Y_{\mathcal{P}}$ ,  $Y_{\mathcal{F}}$ ,  $Y_{\mathcal{P}}^+$  and  $Y_{\mathcal{F}}^-$  are defined similarly to the input block Hankel matrices. Likewise, the block Hankel matrices  $Y_{0|2i-1}^d$  and  $Y_{0|2i-1}^s$  are also defined similarly using the deterministic and stochastic output matrices, respectively. The block Hankel matrices consisting of inputs and outputs as  $W_{0|i-1}$  is defined in (15).

$$\begin{aligned} W_{0|i-1} &\stackrel{\text{def}}{=} \begin{pmatrix} U_{0|i-1} \\ Y_{0|i-1} \end{pmatrix} \\ &= \begin{pmatrix} U_{\mathcal{P}} \\ Y_{\mathcal{P}} \end{pmatrix} \\ &= W_{\mathcal{P}} \end{aligned} \quad (15)$$

Similarly,  $W_{\mathcal{P}}^+ = \begin{pmatrix} U_{\mathcal{P}}^+ \\ Y_{\mathcal{P}}^+ \end{pmatrix}$ .

The state sequence related to the Hankel matrices of the system is defined as (16).

$$\begin{aligned} X_i &\stackrel{\text{def}}{=} (x_i \ x_{i+1} \ \dots \ x_{i+j-2} \ x_{i+j-1}) \\ &\in \mathbb{R}^{n \times j} \end{aligned} \quad (16)$$

Likewise, the deterministic state sequence  $X_i^d$  and stochastic state sequence  $X_i^s$  are defined as (17).

$$\begin{aligned} X_i^d &\stackrel{\text{def}}{=} (x_i^d \ x_{i+1}^d \ \dots \ x_{i+j-2}^d \ x_{i+j-1}^d) \\ &\in \mathbb{R}^{n \times j} \\ X_i^s &\stackrel{\text{def}}{=} (x_i^s \ x_{i+1}^s \ \dots \ x_{i+j-2}^s \ x_{i+j-1}^s) \\ &\in \mathbb{R}^{n \times j} \end{aligned} \quad (17)$$

Hankel block matrices allow calculation of the row space of a Kalman filter state sequence and the column space of the extended observability matrix  $\Gamma_i$  right from

the input-output data (Zhou et al., 2006). Therefore, the oblique projection  $\mathcal{O}_i$  is described as in (18).

$$\mathcal{O}_i \stackrel{\text{def}}{=} Y_{\mathcal{F}} / U_{\mathcal{F}} \mathbf{W}_{\mathcal{P}} \quad (18)$$

However, the matrix  $\mathcal{O}_i$  is equal to the product of the extended observability matrix  $\Gamma_i$  and the Kalman filter state sequence  $\tilde{X}_i$  as depicted in (19) (Makolo, et. al., 2021a) (Isermann & Münchhof, 2010).

$$\mathcal{O}_i = \Gamma_i \cdot \tilde{X}_i \quad (19)$$

Besides, the Kalman filter state sequence  $\tilde{X}_i$  is specified as in (20).

$$\tilde{X}_i \stackrel{\text{def}}{=} \hat{X}_{i|\hat{X}_0} \quad (20)$$

where  $\hat{X}_0 = X_{\mathcal{P}}^d / U_{\mathcal{F}} \mathbf{U}_{\mathcal{P}}$ . Also, the observability matrix  $\Gamma_i$  is given by  $\Gamma_i = W_1^{-1} U_1 S_1^{\frac{1}{2}} T$ .

The part of the state sequence  $\tilde{X}_i$  that lies in the column space of  $W_2$  can be recovered from (21).

$$\tilde{X}_i W_2 = T^{-1} S_1^{\frac{1}{2}} V_1^T \quad (21)$$

It is clear that the Kalman state sequence can also be defined by (22), which can simplify the model identification procedure.

$$\tilde{X}_i = \Gamma_i^{\dagger} \mathcal{O}_i \quad (22)$$

The goal of the model identification procedure is to find an optimal model in which the input-output data approximates the process under consideration. To do this, the prediction of the future outputs ( $Y_{\mathcal{F}}$ ) can be achieved using the information obtained from the past ( $\mathbf{W}_{\mathcal{P}}$ ) and the knowledge of the inputs that will be presented to the system in the future ( $U_{\mathcal{F}}$ ). Predicting future outputs ( $Y_{\mathcal{F}}$ ) helps forecast other network parameters. Inspired by the linearity approximation of the system, the past ( $\mathbf{W}_{\mathcal{P}}$ ) and the future inputs ( $U_{\mathcal{F}}$ ) can be combined linearly to predict the future outputs ( $Y_{\mathcal{F}}$ ). If the linear combination is denoted as  $L_{\mathcal{P}}$ , the optimal combination of the past to predict the future is  $L_{\mathcal{P}} \cdot \mathbf{W}_{\mathcal{P}}$ , which is exactly equal to the oblique projection  $\mathcal{O}_i = L_{\mathcal{P}} \cdot \mathbf{W}_{\mathcal{P}}$  (Isermann & Münchhof, 2010).

To determine states  $\tilde{X}_i$  from the system data collected, the oblique projection in (23) can be used (Zhou et al., 2006).

$$\mathcal{O}_{i+1} = Y_{\mathcal{F}}^- / U_{\mathcal{F}}^- \mathbf{W}_{\mathcal{P}}^+$$

$$\mathcal{O}_{i+1} = \Gamma_{i+1} \cdot \tilde{X}_{i+1} \quad (23)$$

In this way,  $\tilde{X}_i$  and  $\tilde{X}_{i+1}$  can be obtained. However, this new Kalman filter sequence  $\tilde{X}_{i+1}$  has a different initial state from the sequence  $\tilde{X}_i$ . In this way, matrices  $A, B, C$  and  $D$  can be finally obtained as of the set of linear equations of (24).

$$\begin{pmatrix} \tilde{X}_{i+1} \\ Y_{i|i} \end{pmatrix} = \begin{pmatrix} A & B \\ C & D \end{pmatrix} \begin{pmatrix} \tilde{X}_i \\ U_{i|i} \end{pmatrix} + \begin{pmatrix} \rho_{\omega} \\ \rho_v \end{pmatrix} \quad (24)$$

where  $\rho_{\omega}$  and  $\rho_v$  are Kalman filter residuals associated to process and measurement noises of the system. The discussion is mainly based on the system matrix  $A$  as it describes the system's dynamics as characterized by its eigenvalues. Therefore, the system modes have to be obtained by calculating the eigenvalues of the matrix  $A$ , which are the system's poles.

### Online inertia extraction and tracking

An interesting interpretation of system dynamic behaviour can be obtained by analysing the eigenvalues of a dynamic matrix  $A$  of the identified power system model. The system matrix  $A$  is of interest as it describes the system's dynamics as characterized by its eigenvalue structure. The dynamic modes of the system must be found (Makolo, et. al., 2021a) to analyse the system's dynamics. The next step is to obtain the eigenvalues of matrix  $A$ , which are the system's poles.

Considering that the input  $u_k$  is always the same during the experiment, the Kalman residual process noise  $\rho_{\omega}$  in (24) can be estimated to a zero mean, and the block Hankel matrix  $U_{i|i}$  can asymptotically resolve to zero. In this way, the dynamic matrix  $A$  in (24) can be represented by an estimated general form of a dynamic system as (25).

$$\tilde{X}'_{i+1} = A' \tilde{X}'_i \quad (25)$$

where  $\tilde{X}'_{i+1}$  and  $\tilde{X}'_i$  represent estimated Kalman filter state sequences, and  $A'$  represents the estimated dynamic state matrix. If it is assumed that matrix  $A'$  is diagonalisable with eigenvalue decomposition, Kalman filter sequences can be estimated as in (26).

$$\tilde{\mathbf{X}}'_i = \Phi \Lambda \tilde{\Gamma}_m \quad (26)$$

where  $\Phi$  is a set of functions obtained from the system data, which physically represent standing oscillations of the system,  $\tilde{\Gamma}_m$  represents row vectors containing the temporary coefficient evaluated at each observation and  $\Lambda = \text{diag}[\lambda_1 \ \lambda_2 \ \dots \ \lambda_m] \in \mathbb{R}^{m \times m}$  is a diagonal matrix consisting of empirical Ritz eigenvalues  $\lambda_j$  of dynamic matrix  $\mathbf{A}'$  (Barocio *et. al.*, 2015). Therefore, the estimated Kalman sequence matrix  $\tilde{\mathbf{X}}'_i$  can be expanded in a linear combination of modal components (27).

$$\tilde{\mathbf{X}}'_i \approx \sum_{j=1}^m \phi_j \lambda_j \tilde{\mathbf{a}}_j(t) \quad (27)$$

where  $\tilde{\mathbf{a}}_j$  contains the temporal amplitudes,  $\phi_j$  contains the dynamic modes, while  $\lambda_j$  contains the associated eigenvalues of dynamic matrix  $\mathbf{A}'$  of the system model. In this way, eigenvalues and vectors of the state matrices can then be found.

Since system dynamics depend on eigenvalue and eigenvector, any change in dynamic parameters can indirectly change the eigenvalue and eigenvector through the Kalman state sequence matrix. By determining the modes of the system by calculating the eigenvalues of the dynamic matrix  $\mathbf{A}'$ , parameters of the system, such as inertia, can be determined by connecting the eigenvalue of the dynamic matrix  $\mathbf{A}'$  with a linearized form of the swing equation (28).

$$2H\Delta\dot{\omega} + D\Delta\omega = -P_e \quad (28)$$

The related transfer function of the swing equation is given in (29).

$$G(s) = \frac{\Delta\omega}{\Delta P_e} \approx -\frac{1}{2Hs + D} \quad (29)$$

When the system's output is presented at a continuous sampling rate  $\Delta t$ , the sampled signal is represented as per (30).

$$y_j(k) = \sum_{i=1}^n R_i z_i^k \quad (30)$$

where  $k$  shows the samples, and  $z_i = \exp(\lambda_i \Delta t)$  presents the discretized model

variable  $z(t)$  and  $\lambda = \sigma + j\omega$ . These are the modes that represent the system. The set of snapshot matrix of  $\mathbf{A}'$  representing the dynamic modes of the system is given by (31) (Barocio *et al.*, 2015).

$$X = [\Delta f \ \Delta P_e]^T \in \mathbb{R}^{2 \times N} \quad (31)$$

The snapshot matrix (31) can further be evaluated as presented in (Makolo, *et. al.*, 2021a) by means of a linear combination factor (LCF)  $\alpha_i$  to obtain (32).

$$2H\alpha_{i,\Delta f} \lambda \mathcal{b} = -\alpha_{i,\Delta P_e} \mathcal{b}_i \omega_0 \quad (32)$$

in which  $\mathcal{b}_i$  represents the primary value factor corresponding to the  $i^{th}$  eigenvalue. To estimate the inertia, the deviations in power and frequency response deviations are recorded as network's input ( $u_k$ ) and output ( $y_k$ ) regarding the sampled data. The dynamic modes relating to eigenvalues and eigenvectors are then extracted to build the snapshot matrix. Thus, the effective inertia  $H_e$  can be determined by solving equation (32). Given that the equation is linear and lacks a rotor speed derivative, the proposed method is well-suited to handling large-scale power systems with high dimensionality.

### Inertia tracking and forecasting

From the previous subsection, the  $H_e$  of the network is extracted and stored in a dataset with a time interval of 10 s. The stored inertia data create a historical time-series data set. Historical data can potentially be used to form recognizable patterns, such as trends and seasonal events, which are important inputs for long-range forecasting. An appropriate time-series dynamic model is fitted in the stored historical inertia data set. The obtained fitted dynamic model is then used to generate forecasts of future observations. Figure 1 shows the concept of moving observant predictor  $\mathfrak{P}$  for a dynamic forecasting model to forecast future inertia values.

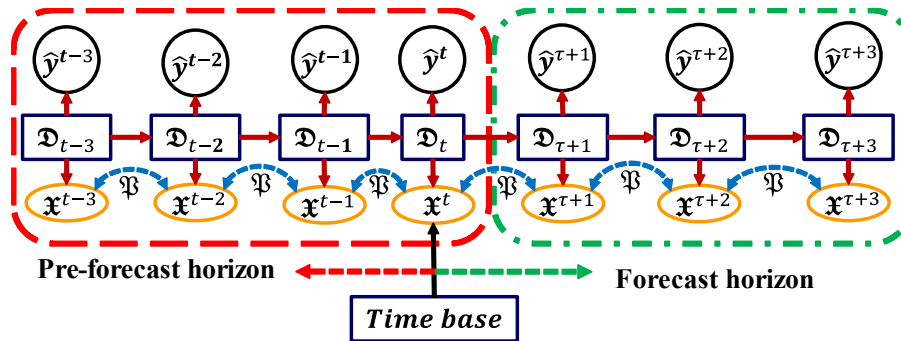


Figure 1: Diagram showing moving observant predictor  $\mathfrak{P}$  in the dynamic forecasting model.

**Inertia tracking**

A time-series data-based ARIMA (p,d,q) process at time  $T + \tau$  is expressed as (33) (Montgomery et. al., 2015).

$$y_{T+\tau} = \delta + \sum_{i=1}^{p+d} \phi_i y_{T+\tau-i} + \varepsilon_{T+\tau} - \sum_{i=1}^q \theta_i \varepsilon_{T+\tau-i} \quad (33)$$

here,  $\delta$  is a data initialization constant,  $\phi_i$  represents the correlation constant between adjacent datasets,  $\varepsilon_{T+\tau}$  denotes the forecast error at lead time  $\tau$ , and  $\theta_i$  is the error correction factor at lead time  $\tau$ . Considering a partitioned MA representation of (33), equation (34) is obtained.

$$y_{T+\tau} = \mu + \sum_{i=0}^{\tau-1} \psi_i \varepsilon_{T+\tau-i} + \sum_{i=\tau}^{\infty} \psi_i \varepsilon_{T+\tau-i} \quad (34)$$

The component  $\sum_{i=0}^{\tau-1} \psi_i \varepsilon_{T+\tau-i}$  represents the future errors, while  $\sum_{i=\tau}^{\infty} \psi_i \varepsilon_{T+\tau-i}$  represents the present and past errors. As the extraction of the inertia is done in the network, the moving average  $MA(q + 1)$  property of the ARIMA model presented in (36) is a powerful property that can be used to track the extracted inertia values. As the inertia series extracted is non-invertible, the maximum likelihood estimates move with the  $q^{\text{th}}$ -order of the MA component, enhancing tracking of the time-changing inertia in the network. The extracted inertia values are compared with the available actual inertia values of the network.

**Short-range forecasting**

On the other side, when the disturbances are assumed to have mean zero and independent on different lags, the forecast estimation at the time ahead  $\tau$  by considering the moving observant predictor  $\mathfrak{P}$  is depicted by (35) (Isermann & Münchhof, 2010).

$$(\hat{y}_{T+\tau}(T))^{\mathfrak{P}} = \left( \sum_{i=\tau}^{\infty} \psi_i \varepsilon_{T+\tau-i} \right)^{\mathfrak{P}} \quad (35)$$

where  $E[y_{T+\tau}|y_T, y_{T-1}, \dots] = \begin{cases} 0 & \text{if } i < \tau \\ \varepsilon_{T+\tau-i} & \text{if } i \geq \tau \end{cases}$

Then, the improved forecast error when  $\mathfrak{P}$  is considered around the historical data is calculated as in (36).

$$(e_T(\tau))^{\mathfrak{P}} = \left( \sum_{i=0}^{\tau-1} \psi_i \varepsilon_{T+\tau-i} \right)^{\mathfrak{P}} \quad (36)$$

For a linear combination of random disturbances,  $E[e_T(\tau)] = 0$ . Therefore, equation (37) is obtained.

$$= (\sigma^2)^{\mathfrak{P}} \sum_{i=0}^{\tau-1} (\psi_i^2)^{\mathfrak{P}} = (\sigma^2)^{\mathfrak{P}}(\tau), \quad \tau = 1, 2, \dots \quad (37)$$

The forecast error variance gets bigger with increasing the forecast lead times  $\tau$ . This increase is expected and makes sense as uncertainty increases for the forecasts further into the future.

### Long-range forecasting

The property that time-series data have strong periodic patterns and seasonality can be used as a crucial input to improve the ARIMA model for long-range forecasting. The improvement is done by including an additive model and exponential smoothing, which are linked by a moving observant predictor  $\mathfrak{P}$  at different lags  $k$  for  $n$  samples of the dataset before and after the time base. For this case, data  $y_t$  can be represented using the additive model as in (38).

$$y_t = S_t + N_t \quad (38)$$

where  $S_t$  is a deterministic component with periodicity and seasonality factor  $s$  in the time-series dataset, while  $N_t$  is a component that may be modelled as the ARIMA process. Equation (38) can further be modified into (39).

$$w_t = (1 - B^s)N_t \quad (39)$$

where  $w_t$  is a process with predictable periodic behaviour, and  $1 - B^s$  is an

operator. On the other hand, using the Holt-Winters method (Chatfield & Yar, 1991), a seasonal with time trend effects exponential smoothing approach for parameters before base time is optimal for an  $ARIMA(0,1, s + 1) \times (0,1,0)_s$ . The exponential smoothing can be improved using the moving observant predictor in line with the additive model for  $n$  sampled parameters to extend the forecasting for long ranges with improved accuracy. Therefore, the improved ARIMA for  $n$  correlated smoothing factor is given by  $ARIMA(0,1, s + 1)_n \times (0,1,0)_s^{\mathfrak{P}}$ . This improved ARIMA model for long-range forecasting is referred to as  $i$ -ARIMA.

The proposed method is summarized by algorithms that are classified into three parts: inertia monitoring, extraction, and forecasting, as demonstrated in Algorithm 1, Algorithm 2, and **Error! Reference source not found.**, as presented in Table 1, Table 2 and Table 3, respectively.

**Table 1: Algorithm 1: Network Model Identification**

| Part I: Network Model Identification |  |
|--------------------------------------|--|
| 1.                                   | <b>Input:</b> Aggregated Power deviation of the network ( $\mathbf{u}_k = \Delta P$ )  |
| 2.                                   | <b>Output:</b> Frequency response deviations at the centre of inertia, ( $\mathbf{y}_k = \Delta \omega$ )  |
| 3.                                   | <b>State-space model:</b>  |
|                                      | $x_{k+1} = Ax_k + Bu_k + w_k$ $y_k = Cx_k + Du_k + v_k$  |
| 4.                                   | <b>Block Hankel:</b> Generate input and output block Hankel, extended block Hankel matrices, as well as past and future matrices using input-output data vectors, $\mathbf{u}_k, \mathbf{y}_k$                       |
| 5.                                   | <b>Oblique projection:</b> Compute the oblique and orthogonal projections using block Hankel matrices  |
|                                      | $\mathcal{O}_i \stackrel{\text{def}}{=} Y_f / U_f W_p$ $\mathcal{O}_{i+1} = Y_f^- / U_f^- W_p^+$   |
| 6.                                   | <b>SVD:</b> Compute the SVD of the subjective oblique projection using   |
|                                      | $W_1 \mathcal{O}_i W_2 = USV^T$  |
| 7.                                   | <b>Kalman sequence:</b> Determine the Kalman state sequences   |
|                                      | $\tilde{X}_i = \Gamma_i^\dagger \mathcal{O}_i$ $\tilde{X}_{i+1} = \Gamma_{i-1}^\dagger \mathcal{O}_{i+1}$  |
| 8.                                   | <b>Dynamic matrix A:</b> Compute the equations for A, B, C and D   |
|                                      | $\begin{pmatrix} \tilde{X}_{i+1} \\ Y_{i i} \end{pmatrix} = \begin{pmatrix} A & B \\ C & D \end{pmatrix} \begin{pmatrix} \tilde{X}_i \\ U_{i i} \end{pmatrix} + \begin{pmatrix} \rho_\omega \\ \rho_v \end{pmatrix}$ |
| 9.                                   | <b>Pass</b> on the dynamic matrix <b>A</b> to the next algorithm   |

**Table 2: Algorithm 2: Inertia extraction**

| <b>Part II: Inertia extraction from dynamic matrix A</b> |  |
|--|--|
| 1.   | <b>Eigenstructure:</b> Calculate the eigenvectors and eigenvalues of the system by solving the characteristic equation of the dynamic matrix <b>A</b> .<br>$\begin{aligned}\tilde{X}'_{i+1} &= A' \tilde{X}'_i \\ A\vec{V} &= \lambda\vec{V}\end{aligned}$           |
| 2.   | <b>Kalman matrix:</b> Obtain the Kalman sequence matrix $\tilde{X}'_i$ as<br>$\tilde{X}'_i \approx \sum_{j=1}^m \phi_j \lambda_j \tilde{a}_j(t)$   |
| 3.   | <b>Snapshot matrix:</b> Determine the snapshot matrix of the estimated dynamic matrix <b>A'</b> representing the dynamic modes of the system.<br>$X = [\Delta f \ \Delta P_e]^T \in \mathbb{R}^{2 \times N}$   |
| 4.   | <b>Inertia extraction:</b> Obtain the estimated system inertia by identifying the dynamic mode associated with the eigenvalue that corresponds to the system's inertia.<br>$2H\alpha_{i,\Delta f} \lambda \mathcal{B} = -\alpha_{i,\Delta P_e} \mathcal{B} \omega_0$ |
| 5.   | <b>Pass on the extracted inertia to the next algorithm</b>   |

**Table 3: Algorithm 3: Inertia forecasting**

| <b>Part III: Inertia tracking and forecasting</b> |  |
|---|--|
| 1.  | <b>Time-series:</b> Generate historical time series data sets of the extracted inertia values from the network model.  |
| 2.  | <b>ACF &amp; PACF:</b> Obtain Autocorrelation function (ACF) and partial autocorrelation function (PACF).<br>$\rho_y(k) = \frac{\gamma_y(k)}{\gamma_y(0)}$   |
| 3.  | <b>Check stationarity:</b> Based on ACF and PACF, the stationarity of the time series data set is checked.<br>$Cov(y_t, y_{t+k}) = \sum_{i=-\infty}^{\infty} \sum_{j=-\infty}^{\infty} \psi_i \psi_j \gamma_x(i - j + k)$  |
| 4.  | <b>Fit ARIMA model:</b> An ARIMA (p,d,q) is fitted on the checked data set and based on the moving average component of ARIMA, the inertia data are tracked.   |
| 5.  | <b>Forecast:</b> Develop forecast models for short- and long-range forecasting of inertia values.<br>$\begin{aligned}(\hat{y}_{T+\tau}(T))^{\mathfrak{P}} &= \left( \sum_{i=\tau}^{\infty} \psi_i \varepsilon_{T+\tau-i} \right)^{\mathfrak{P}} \\ &ARIMA(0,1, s+1)_n \times (0,1,0)_s\end{aligned}$ |
| 6.  | <b>Validate:</b> The forecasting model's accuracy performances are tested and validated using the appropriate validating metrics.<br>$MAPE = \frac{1}{N} \sum_{t=1}^N \left  \frac{y_t - \hat{y}_t}{y_t} \right $  |

**APPLICATION ON THE DATA FROM NEW ZEALAND GRID**

**Data preparation and processing**

The time series representing the power profiles for the years 2018 to 2022 is

presented in Figure 2. In this power profile, the time resolution is 30 minutes, as obtained from New Zealand's Electricity Authority webpage (Hiko, 2021). Figure 2 (a) shows the total power profile in the network, Figure 2

(b) shows the power profile for total renewable power contribution in the network, and Figure 2 (c) represents the contribution of wind power in the network. It can further be noted that the presented power profiles follow strong periodic and seasonality patterns.

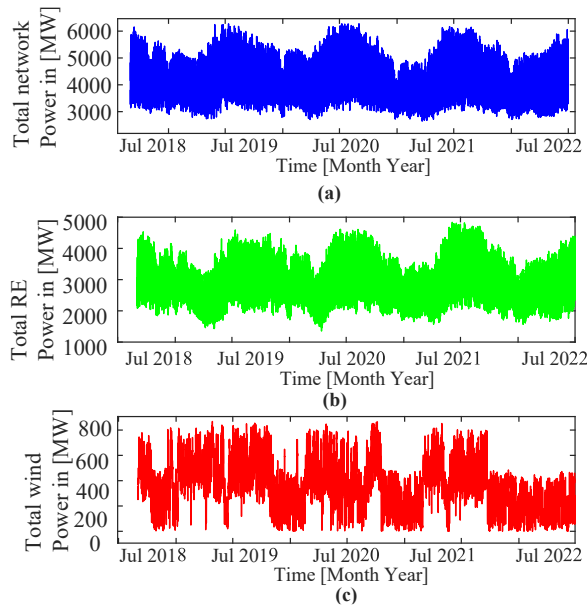


**Figure 2: New Zealand power profiles for the years 2018 to 2022.**

Since inertia is at the core of the discussion, the suggested approach is verified by analysing and digesting the available data. With the SCADA data acquired from Transpower, the time series for the network's total inertia values are generated, allowing for the determination of when a generator was synchronised to the grid. Transpower's report provides the inertia values for every generator. (Transpower, 2014). Equation (7) is used to derive the time series inertia of the network and is presented with a time resolution of 10 seconds. Figure 3 (a) presents the time-series inertia of the network in (s), while Figure 3 (b) represents the time-series of the combined kinetic energy of the interconnected synchronous generators in (MWs).

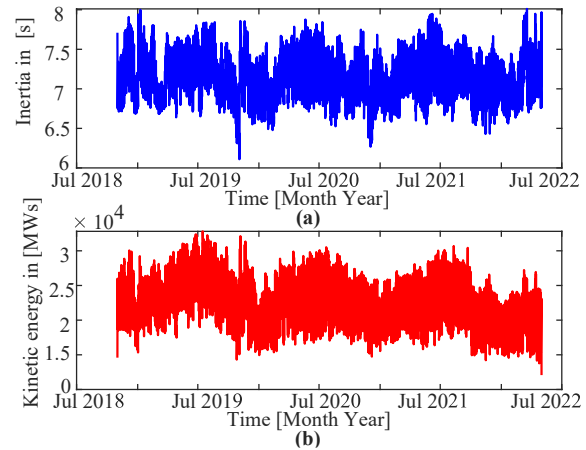


**Figure 3: (a) Time series of inertia in (s) and (b) Aggregated kinetic energy in (MWs) of the New Zealand network**

### Checking the stationarity of the data

After obtaining the time-series data profiles of power generation and the inertia of the network for the years under consideration, a stationarity check is carried out to identify the stationarity status of the time-series data profile of inertia. ACF and PACF at different lags plots are obtained to check the stationarity of the time-series data. The ARIMA (1,1,1) can be used for stationary time series data to estimate, analyse and forecast observations based on the presented time series data. For the ARIMA (1,1,1) model, the order of autoregression (AR) is one, integrator (I) is one, and the moving average (MA) is one. With the moving average, the ARIMA (1,1,1) model can also be used to track the presented time series data. From ACF and PACF, stationary time-series data is identified. As the presented time series data satisfy the stationarity conditions, the ARIMA (1,1,1) is fitted on the inertia time-series data from October – December 2022 to represent the rest of the data. Figure 4 shows how the ARIMA (1,1,1) model fits the data for 98% in (a), which is further proven with the residual index plot in (b).

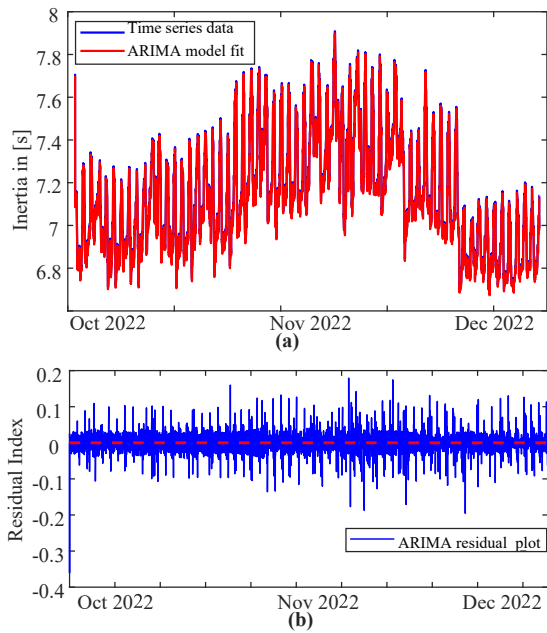


**Figure 4: (a) ARIMA (1,1,1) model fitting historical data set by 98%, (b) Residual index plot.**

### Inertia tracking

The proposed technique tracks the dynamics of inertia values in the network using the created time-series data. The method's tracking speed is so fast that, when inertia changes, it only takes  $25\mu\text{s}$  for the estimation from the improved moving average (MA) of the ARIMA model to track the actual inertia signal. Evidence is shown in Figure 5 (a) when tracking is done for the data set of one month. The figure displays the network's inertia dynamics during a one-month period in (s). A few data sets are used to observe the efficacy of the proposed scheme closely. A week's worth of data is used to test the procedure in Figure 5 (b) (seven days). It is evident how well the ARIMA model's enhanced MA tracks the original inertia signal. In addition, Figure 5 (c) provides a close-up and clear perspective by zooming in on the tracking for two days.

Next, the method is tested on the network data using stored kinetic energy in [MWs]. Figure 6 (a) presents a one-month data set to represent the data. Similar to inertia in (s), a small range of data is used to highlight the efficacy of the technique. Therefore, Figure 6 (b) presents the tracking of the stored kinetic inertia of the network for a ten-day data set.

Figure 7 (a) and Figure 7 (b) show the tracking of the stored kinetic energy of the network for seven days and two days data sets, respectively. From the view in the figure, it is clear that the proposed tracking method monitors the stored kinetic energy effectively.

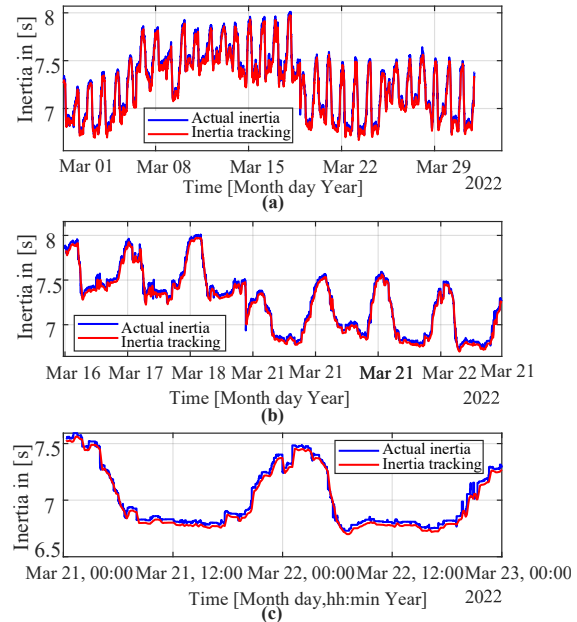


**Figure 5: (a), (b) and (c) Tracking of inertia for one month, one week and two days, respectively**

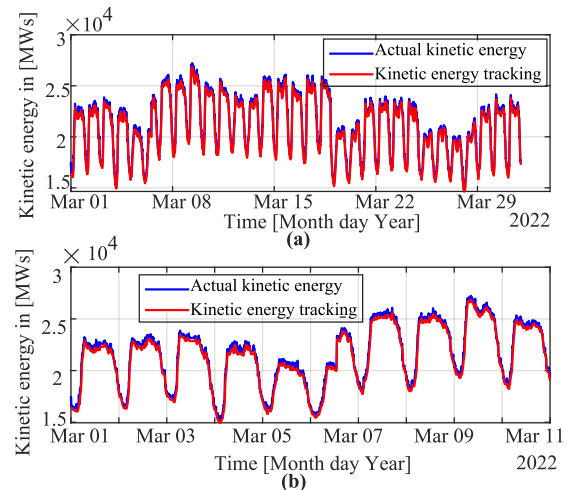


**Figure 6: (a) Tracking of inertia data for one month. (b) Tracking of inertia data for one week**

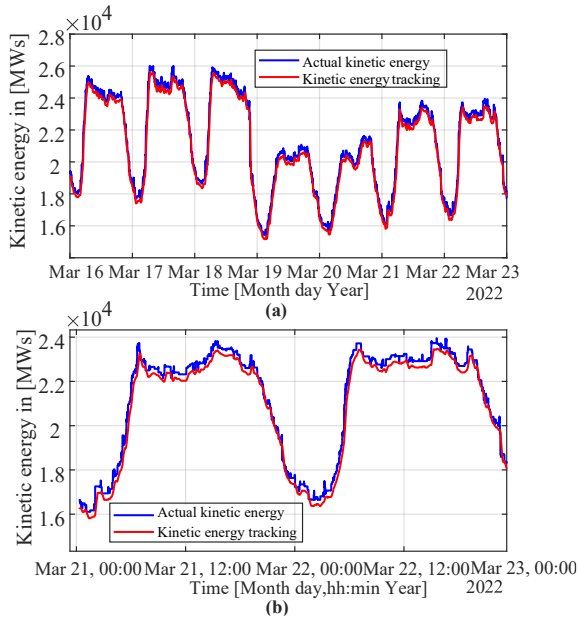


Figure 7: (a) and (b) Tracking of kinetic energy for one week and two days, respectively

### Inertia forecasting

The suggested method is tested for the time ahead prediction of the total system inertia in (s) and the kinetic inertia of the network in (MWs). The historical measurement data provided in the preceding subsection verify the proposed technique. Tests are conducted on the proposed approach over various time horizons, categorised as short- and long-range forecasting. The results are compared with other forecasting methods from (Carlini *et al.*, 2021; Paidi *et al.*, 2020). The performance of the forecasting methods to be compared is tested on the actual New Zealand network data. The various time horizon forecasts are tested at various intervals ahead of the current moment.

The method is tested for the seven-day time ahead forecasting, as observed in Figure 8 (a). The results are not good as the forecasting error is outside the acceptable range, according to (Wambura *et al.*, 2020). Therefore, further investigation is done to identify the longest time ahead for which the proposed method can give results with acceptable forecasting errors. Finally, the optimal time ahead is identified to be a maximum of two days ahead, as presented in Figure 8 (b).

The method is also tested for the network's stored kinetic energy, just like for inertia.

Figure 9 (a) illustrates the seven-day test run of the approach. Lastly, as shown in Figure 9 (b), the ideal maximum predicting time yielding a reasonable variance is again restricted to two days.

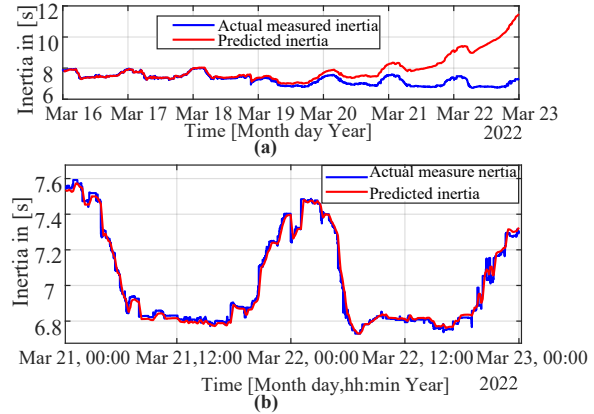


Figure 8: (a) and (b) Inertia forecasting for seven days and two days, respectively

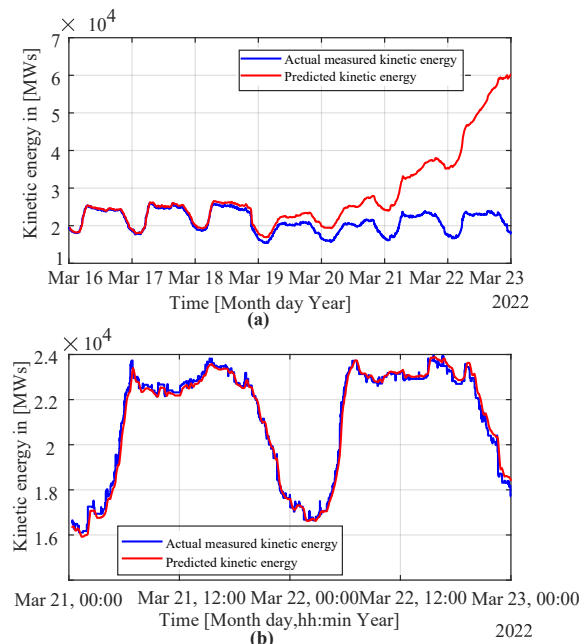


Figure 9: (a) and (b) Kinetic energy forecasting for seven days and two days, respectively

### PERFORMANCE ANALYSIS OF THE PRESENTED TECHNIQUE

The widely used metrics to evaluate forecasting methods are mean square error (MSE), root mean square error (RMSE), mean absolute percentage error (MAPE) and mean absolute error (MAE). However, due to some denunciations that these metrics are undefined in some cases (Wambura *et al.*, 2020; Chen *et al.*, 2017), the performance

accuracy and quality for short-range are evaluated using symmetric mean absolute error (SMAE). This metric is defined as in (40).

$$SMAE = \frac{1}{N} \sum_{t=1}^N \left\{ \frac{|y_t - \hat{y}_t|}{|y_t| + |\hat{y}_t|} \right\} \quad (40)$$

where  $N$  denotes the number of experimental data,  $y_t$  and  $\hat{y}_t$  are the true and predicted inertia at  $t^{th}$  time, correspondingly. On the other hand, due to the fact that SMAE can be used for long-range forecasts, the long-range forecast performance accuracy and quality are still checked by MAPE. The MAPE metric is defined as in (41).

$$MAPE = \frac{1}{N} \sum_{t=1}^N \left| \frac{y_t - \hat{y}_t}{y_t} \right| \quad (41)$$

The performance superiority of the technique is tested in reference to the other two different forecasting methods presented in (Carlini et al., 2021; Paidi et. al., 2020). Testing and comparing the proposed methods is conducted using historical inertia data for the New Zealand network to validate the method. The testing is conducted to examine the important aspects of modern power systems application: accuracy, robustness, time horizon and speed of communication to the PSOs. While examining these features, other aspects, such as uncertainty and dormant historical patterns in the data, are considered. The presented power and inertia data in Figure 2 and Figure 3 show that the datasets' characteristics can be autoregressive, moving average and seasonal (Montgomery et. al., 2015). The repeating patterns observed in historical datasets covering a long time, such as for a few years, help the moving observant predictor to forecast the data trends for long ranges. Using the stationarity factor in data allows the proposed method to cope with stochasticity in datasets with well-standardized uncertainty estimates (Montgomery et. al., 2015).

### Online tracking

To evaluate the accuracy of the tracking capability, the improved moving average window in the ARIMA model is used to track inertia measurements from the network. As presented in the given inertia data with a time resolution of 10 sec, the algorithm gets enough time to prepare and track the next observation measurement with a speed of  $25\mu s$  and a refresh rate of 2 s. A statistical analysis is carried out for each set of estimation data obtained at different levels of RES penetration. As shown in Figure 5 to Figure 7, the tracking signal tracks/monitors effectively the actual system inertia signal throughout the data presented.

### Short-range forecasting

The proposed method is tested for a short time ahead of the network inertia forecasting. In this case, the time ahead is limited to only four hours. The comparison methods are also applied to four-hour time ahead forecasting tested on New Zealand data. **Error! Reference source not found.** The applicability comparison of the proposed method with the other two methods as measured by SMAE on various datasets are presented on Table 4. The proposed method gives superior results over the other competing methods.

**Table 4: Comparison of SMAE between the proposed method and the two other forecasting methods**

| Technique                           | SMAE         |
|-------------------------------------|--------------|
| <i>i</i> -ARIMA technique           | <b>0.051</b> |
| Artificial Neural Network technique | 0.101        |
| MVHFIR technique                    | 0.130        |

**Error! Reference source not found.**5 also gives a further SMAE comparison of the proposed technique to other forecasting methods (method 1 in Carlini et. al., 2021 and method 2 in Prakash et al., 2018) for the specific different time ahead forecasts. For a maximum of four hours of the forecast, the proposed method has better accuracy for each step of the time ahead forecast.

**Table 5: SMAE comparison of the proposed method to other two forecasting methods across various forecast lead times**

| Time (hr) | SMAE            |          |          |
|-----------|-----------------|----------|----------|
|           | Proposed method | Method 1 | Method 2 |
| 0.0       | 0.001           | 0.015    | 0.005    |
| 0.5       | 0.003           | 0.021    | 0.009    |
| 1.0       | 0.005           | 0.028    | 0.014    |
| 1.5       | 0.008           | 0.034    | 0.022    |
| 2.0       | 0.010           | 0.039    | 0.031    |
| 2.5       | 0.017           | 0.051    | 0.045    |
| 3.0       | 0.022           | 0.067    | 0.052    |
| 3.5       | 0.028           | 0.083    | 0.064    |
| 4.0       | 0.035           | 0.110    | 0.078    |

The trend of the proposed method on the test data demonstrates the forecasting power of the proposed method in capturing essential dynamic features of the effective inertia in the considered network. For the considered short time, the comparing forecast methods hardly performed better. The influence of the moving observant predictor gives the proposed method an advanced performance as it improves the forecast time horizon, accuracy and robustness to variations in inertia and prevalent patterns. The predictor further reduces prediction variances and gives better probabilistic outputs with reduced residual errors.

### Long-range forecasting

The *i*-ARIMA is further tuned for different values of moving observant predictor  $\mathfrak{P}$ , periodicity and seasonality factor of the time-series data set  $s$  and the smoothing factor  $n$ . After several tunings, the five combinations of the parameters that give good forecasts and accuracy for one-hour forecasts in terms of MAPE [%] are presented in Table 5. The optimal combination values that give the best forecasts and accuracy are 0.235, 10 and 17 for  $\mathfrak{P}$ ,  $s$  and  $n$ , respectively, as shown in Table 6. Using this combination, the method is tested for one day ahead forecast and then for two days ahead forecast. The proposed method does very well for a day-ahead forecast of the network inertia, giving MAPE of 3.06%. It also gives good forecasts for 48 hours with the maximum MAPE of 8.89% before the accuracy reduces significantly for

further predictions of the inertia values beyond 48 hours. Because of this, the proposed approach is the most effective way to predict long-range inertia values in contemporary power systems.

**Table 6: Tuned moving observant predictor  $\mathfrak{P}$ , periodicity and seasonality factor  $s$  and the smoothing factor  $n$  for best forecasts**

| Tuning score | $\mathfrak{P}$ | $s$       | $n$       | MAPE        |
|--------------|----------------|-----------|-----------|-------------|
| 1            | <b>0.235</b>   | <b>10</b> | <b>17</b> | <b>1.23</b> |
| 2            | <b>0.341</b>   | <b>12</b> | <b>16</b> | <b>3.41</b> |
| 3            | 0.862          | 11        | 15        | 6.82        |
| 4            | 0.541          | 14        | 16        | 8.11        |
| 5            | 0.439          | 9         | 14        | 12.97       |

### CONCLUSION

This paper presents an effective and improved ARIMA framework termed *i*-ARIMA that forecasts a network's short- and long-range inertia values. The approach uses the power of strong periodic and seasonality patterns of the time series data to introduce a moving observant predictor at different lags to give it a superior capability for long-range inertia forecast in power systems. The best accuracy of the *i*-ARIMA is achieved by fine-tuning and selecting the optimal combination of the moving observant predictor, periodicity and seasonality factor and smoothing factor at different lags. Based on previous historical inertia data set observations in the New Zealand network, the *i*-ARIMA is evaluated and tested. The results show that *i*-ARIMA is fast, robust, accurate and superior to other forecasting methods.

### REFERENCES

- Ashton, P. M., Saunders, C. S., Taylor, G. A., Carter, A. M., & Bradley, M. E. (2014). Inertia estimation of the GB power system using synchrophasor measurements. *IEEE Transactions on Power Systems*, **30**(2), 701–709. doi: 10.1109/TPWRS.2014.2333776
- Ashton, P. M., Taylor, G. A., Carter, A. M., Bradley, M. E., & Hung, W. (2013). Application of phasor measurement units to estimate power system inertial

- frequency response. *2013 IEEE Power & Energy Society General Meeting*, 1–5. doi: 10.1109/PESMG.2013.6672671.
- Barocio, E., Pal, B. C., Thornhill, N. F., & Messina, A. R. (2015). A dynamic mode decomposition framework for global power system oscillation analysis. *IEEE Transactions on Power Systems*, **30**(6), 2902–2912. doi: 10.1109/TPWRS.2014.2368078.
- Cao, X., Stephen, B., Abdulhadi, I. F., Booth, C. D., & Burt, G. M. (2016). Switching Markov Gaussian models for dynamic power system inertia estimation. *IEEE Transactions on Power Systems*, **31**(5), 3394–3403. doi: 10.1109/TPWRS.2015.2501458.
- Carlini, E. M., Del Pizzo, F., Giannuzzi, G. M., Lauria, D., Mottola, F., & Pisani, C. (2021). Online analysis and prediction of the inertia in power systems with renewable power generation based on a minimum variance harmonic finite impulse response filter. *International Journal of Electrical Power & Energy Systems*, **131**, 107042. doi: 10.1016/j.ijepes.2021.107042.
- Chassin, D. P., Huang, Z., Donnelly, M. K., Hassler, C., Ramirez, E., & Ray, C. (2005). Estimation of WECC system inertia using observed frequency transients. *IEEE Transactions on Power Systems*, **20**(2), 1190–1192. doi: 10.1109/TPWRS.2005.846155.
- Chatfield, C., & Yar, M. (1991). Prediction intervals for multiplicative Holt-Winters. *International Journal of Forecasting*, **7**(1), 31–37. doi: 10.1016/S0169-2070(01)00081-4.
- Chen, C., Twycross, J., & Garibaldi, J. M. (2017). A new accuracy measure based on bounded relative error for time series forecasting. *PloS One*, **12**(3), e0174202. doi: 10.1371/journal.pone.0174202.
- Donnini, G., Carlini, E., Giannuzzi, G., Zaottini, R., Pisani, C., Chiodo, E., Lauria, D., & Mottola, F. (2020). On the Estimation of Power System Inertia accounting for Renewable Generation Penetration. *2020 AEIT International Annual Conference (AEIT)*, 1–6. doi: 10.23919/AEIT50178.2020.9241204.
- Du, P., & Matevosyan, J. (2017). Forecast system inertia condition and its impact to integrate more renewables. *IEEE Transactions on Smart Grid*, **9**(2), 1531–1533. doi: 10.1109/TSG.2017.2662318.
- Gonzalez-Longatt, F., Acosta, M. N., Chamorro, H. R., & Topic, D. (2020). Short-term Kinetic Energy Forecast using a Structural Time Series Model: Study Case of Nordic Power System. *2020 International Conference on Smart Systems and Technologies (SST)*, 173–178. doi: 10.1109/SST49455.2020.9264087.
- Heylen, E., Strbac, G., & Teng, F. (2020). Challenges and opportunities of inertia estimation and forecasting in low-inertia power systems. *Vol. 147*. doi: 10.1016/j.rser.2021.111176.
- Electricity Authority (Te Mana Hiko), (2021). Generation output by plant. Electricity Authority. [https://www.emi.ea.govt.nz/Wholesale/Datasets/Generation/Generation\\_MD](https://www.emi.ea.govt.nz/Wholesale/Datasets/Generation/Generation_MD)
- Inoue, T., Taniguchi, H., Ikeguchi, Y., & Yoshida, K. (1997). Estimation of power system inertia constant and capacity of spinning-reserve support generators using measured frequency transients. *IEEE Transactions on Power Systems*, **12**(1), 136–143. doi: 10.1109/59.574933.
- Isermann, R., & Münchhof, M. (2010). *Identification of dynamic systems: an introduction with applications*. Vol. 85. Springer Science & Business Media.
- Kisinga, D. A., Makolo, P., & Trodden, P. (2024). A modified synchronverter for a weak grid with virtual power circles - based PQ decoupling scheme. *IET Renewable Power Generation*, **18**(14). doi: 10.1049/rpg2.13118.
- Kosmecki, M., Rink, R., Wakszyńska, A., Ciavarella, R., Di Somma, M., Papadimitriou, C. N., Efthymiou, V., & Graditi, G. (2021). A Methodology for Provision of Frequency Stability in Operation Planning of Low Inertia Power Systems. *Energies*, **14**(3), 737. doi: 10.3390/en14030737.
- Linaro, D., Bizzarri, F., Del Giudice, D., Pisani, C., Giannuzzi, G. M., Grillo, S., & Brambilla, A. M. (2023). Continuous estimation of power system inertia using convolutional neural networks. *Nature Communications*, **14**(1), 4440. doi: 10.1038/s41467-023-40192-2.
- Liu, M., Chen, J., & Milano, F. (2020). On-line Inertia Estimation for Synchronous and Non-Synchronous Devices. *IEEE Transactions on Power Systems*, **36**(3). doi: 10.1109/TPWRS.2020.3037265.
- Lugnani, L., Dotta, D., Lackner, C., & Chow, J. (2020). ARMAX-based method for

- inertial constant estimation of generation units using synchrophasors. *Electric Power Systems Research*, **180**, 106097. doi: 10.1016/j.epsr.2019.106097.
- Makolo, P., Oladeji, I., Zamora, R., & Lie, T.-T. (2021). Short-range Inertia Prediction for Power Networks with Penetration of RES. *TENCON 2021-2021 IEEE Region 10 Conference (TENCON)*, 765–770. doi: 0.1109/TENCON54134.2021.9707270.
- Makolo, P., Oladeji, I., Zamora, R., & Lie, T.-T. (2021). Data-driven inertia estimation based on frequency gradient for power systems with high penetration of renewable energy sources. *Electric Power Systems Research*, **195**, 107171. doi: 10.1016/j.epsr.2021.107171.
- Makolo, P., Zamora, R., & Lie, T. (2021a). Online inertia estimation for power systems with high penetration of RES using recursive parameters estimation. *IET Renewable Power Generation*, **15**(12). doi: 10.1049/rpg2.12181.
- Makolo, P., Zamora, R., & Lie, T.-T. (2021b). The role of inertia for grid flexibility under high penetration of variable renewables—A review of challenges and solutions. *Renewable and Sustainable Energy Reviews*, **147**, 111223. doi: 10.1016/j.rser.2021.111223.
- Makolo, P., Zamora, R., Perera, U., & Lie, T. T. (2024). Flexible Synthetic Inertia Optimization in Modern Power Systems. *Inventions*, **9**(1), 18. doi: 10.3390/inventions9010018.
- Milano, F., Dörfler, F., Hug, G., Hill, D. J., & Verbič, G. (2018). Foundations and challenges of low-inertia systems. 2018 *Power Systems Computation Conference (PSCC)*, 1–25. doi: 10.23919/PSCC.2018.8450880.
- Montgomery, D. C., Jennings, C. L., & Kulahci, M. (2015). *Introduction to time series analysis and forecasting*. John Wiley & Sons.
- Paidi, E. S. N. R., Marzooghi, H., Yu, J., & Terzija, V. (2020). Development and Validation of Artificial Neural Network-Based Tools for Forecasting of Power System Inertia With Wind Farms Penetration. *IEEE Systems Journal*, **14**(4), 4978–4989. doi: 10.1109/JSYST.2020.3017640.
- Panda, R. K., Mohapatra, A., Srivastava, S. C., & Kezunovic, M. (2020). Energy Function based Approach for Online Inertia Estimation Utilizing Synchrophasor Measurements. 2020 *IEEE Texas Power and Energy Conference (TPEC)*, 1–6. doi: 10.1109/TPEC48276.2020.9042566.
- Prakash, V., Bhakar, R., Tiwari, H., & Sharma, K. C. (2018). System Inertia Prediction for Primary Frequency Response Adequacy Under Uncertain Wind Generation. 2018 8<sup>th</sup> *IEEE India International Conference on Power Electronics (IICPE)*, 1–6. doi: 10.1109/IICPE.2018.8709539.
- Ratnam, K. S., Palanisamy, K., & Yang, G. (2020). Future low-inertia power systems: Requirements, issues, and solutions—A review. *Renewable and Sustainable Energy Reviews*, **124**, 109773. doi: 10.1016/j.rser.2020.109773.
- Sfetskos, A. I., Kontis, E. O., Papadopoulos, T. A., & Papagiannis, G. K. (2023). Inertia estimation of multi-area power systems using tie-line measurements and modal sensitivity analysis. *Electric Power Systems Research*, **224**, 109642. doi: 10.1016/j.epsr.2023.109642.
- Sun, M., Feng, Y., Wall, P., Azizi, S., Yu, J., & Terzija, V. (2019). On-line power system inertia calculation using wide area measurements. *International Journal of Electrical Power & Energy Systems*, **109**, 325–331. doi: 10.1016/j.ijepes.2019.02.013.
- Tavakoli, M. R. B., Power, M., Ruttledge, L., & Flynn, D. (2012). Load inertia estimation using white and grey-box estimators for power systems with high wind penetration. *IFAC Proceedings*, **45**(21), 399–404. doi: 10.3182/20120902-4-FR-2032.00071.
- Transpower, & Transpower. (2014). System Operator TASC Report. In TASC 033 report. Transpower. <https://www.transpower.co.nz/sites/default/files/bulk-upload/documents/TASC%20033%20report.pdf>
- Tuttelberg, K., Kilter, J., Wilson, D. H., & Uhlen, K. (2018). Estimation of Power System Inertia from Ambient Wide Area Measurements. *IEEE Transactions on Power Systems*, **33**(6), 7249–7257. doi: 10.1109/TPWRS.2018.2843381
- Ujjwol, T., Dipesh, S., Manisha, M., Bishnu, P. B., Timothy, M. H., & Reinaldo, T. (2017). Virtual Inertia: Current Trends and Future Directions. *Applied Sciences*, **7**(7): 654 (2017) doi: 10.3390/app7070654

- Wambura, S., Huang, J., & Li, H. (2020). Long-range forecasting in feature-evolving data streams. *Knowledge-Based Systems*, **206**, 106405. doi: 10.1016/j.knosys.2020.106405.
- Wang, W., Yao, W., Chen, C., Deng, X., & Liu, Y. (2020). Fast and accurate frequency response estimation for large power system disturbances using second derivative of frequency data. *IEEE Transactions on Power Systems*, **35**(3), 2483–2486. doi: 10.1109/TPWRS.2020.2977504.
- Yang, D., Wang, B., Ma, J., Chen, Z., Cai, G., Sun, Z., & Wang, L. (2020). Ambient-data-driven Modal-identification-based Approach to Estimate the Inertia of an Interconnected Power System. *IEEE Access*, **8**, 118799–118807. doi: 10.1109/ACCESS.2020.3004335
- Zhang, J., & Xu, H. (2017). Online Identification of Power System Equivalent Inertia Constant. *IEEE Transactions on Industrial Electronics*, **64**(10), 8098–8107. doi: 10.1109/TIE.2017.2698414.
- Zhou, N., Pierre, J. W., & Hauer, J. F. (2006). Initial results in power system identification from injected probing signals using a subspace method. *IEEE Transactions on Power Systems*, **21**(3), 1296–1302. doi: 10.1109/TPWRS.2006.879292.
- Zografos, D., Ghandhari, M., & Eriksson, R. (2020). Real Time Frequency Response Assessment Using Regression. 2020 *IEEE PES Innovative Smart Grid Technologies Europe (ISGT-Europe)*, 399–403. doi: 10.1109/ISGT-Europe47291.2020.9248783.